ADVANCED OPTICAL MATERIALS
www.advopticalmat.de

Check for updates

Janus Structural Color from a 2D Photonic Crystal Hybrid with a Fabry–Perot Cavity

Chang Li, Maoxiong Zhao, Xue Zhou, Huizeng Li, Yang Wang, Xiaotian Hu, Mingzhu Li, Lei Shi,* and Yanlin Song*

Structural colors are widely applied for their stability and their sophisticated optical responses. However, these colors always appear washed-out or pale assigning to the defect hardly avoided in the manufacturing procedures. It is still a challenge to bring multifunctional vivid color via a facile method. A composite structure combining 2D photonic crystal and Fabry–Perot cavity by a simple and convenient method is constructed here. Various metallic colors with tunable hue and high saturation are produced by the composite structure. What is more, an obvious optical Janus effect is created by the composite structure. Iridescent colors can be observed when viewing from the same side of incident light but only pale colors can be seen from the opposite side. The hues and saturation of the colors can be adjusted by the parameters of the composite structure. The experimental results indicate that the color is derived from the synergistic effect of the interference, the diffraction, and the Rayleigh scattering of the composite structure. The facile composite photonic structure pioneers a new way for art, architecture, and security features in anticounterfeiting materials.

Structural colors are brilliant and diversified colors are generated by micro-/nanostructures. Compared with the conventional dye/pigment-based colorants, the structural colors deliver conspicuous merits encompassing the cost-effectiveness, environment friendliness, high reproduction fidelity, and sustainability. It has been subject to extensive studies to dig out the color fundamentals in nature[1,2] and to fabricate the artificial colors for growing applications such as painting,[3,4] sensing,[5–7] display technologies,[8,9] and security.[10] In general, structural coloration is usually yielded by the special propagation methods when the light incident onto a special structure[11] including film interference,[3,12] diffraction grating,[13,14] light scattering,[15,16] photonic crystals,[17–19] surface plasmon resonance,[20,21] and so on.[22] Hue and saturation are two crucial factors for color. For the artificial structural color, it is facile to tune the hue by controlling the refractive index of the component materials and the lattice constant of the optical structure. However, the saturation of the color is often reduced because of the hardly avoided defects in the manufacturing process. It is still a big challenge to generate pure structural color with high saturation.[23]

It has been reported that many living organisms can generate vivid colors through the synergistic effect of the sophisticated structures as well as the absorbing elements. Inspired by the natural brilliant colored structures, two strategies are usually utilized to produce pure color: one is the combination of absorbing elements and structural coloration, and the other strategy is to fabricate rational composite structure. It has been widely studied that the absorbing elements can eliminate the incoherent scattering light and result in saturated coloration. Zi and co-workers made amorphous photonic structures by self-assembling the mixture of monodisperse polystyrene (PS) spheres and cuttlefish ink particles which had broadband high absorption.[24] Aizenberg and co-workers purified the spectrum of the structurally colored materials by localizing the plasmonic nanoparticles.[25] Besides the combination of the absorber with the structural color, the irradiant colors induced by the composite nanoscale architectures is another candidate which present some unique optical properties.[26–28] For example, the origin of the bright vivid coloration of the wing scales of the Papilio butterfly is an extraordinary combination of both green and blue iridescence generated by a multilayered structure embedded in 2D arrays of deep concavities.[27] The golden color of *Cosmophasis thalassina* spider is assigned to a combination of a diffraction grating and an underlying broadband multilayer reflector.[28] In addition, the chameleons are endowed with an amazing ability to change their color to imitate any individual

C. Li, X. Zhou, Dr. H. Li, Dr. Y. Wang, X. Hu, Prof. M. Li, Prof. Y. Song
Key Laboratory of Green Printing
CAS Research/Education Center for Excellence in Molecular Sciences
Institute of Chemistry Chinese Academy of Sciences (ICCAS)
Beijing Engineering Research Center of Nanomaterials for Green Printing Technology
National Laboratory for Molecular Sciences (BNLMS)
Beijing 100190, P. R. China
E-mail: mingzhu@iccas.ac.cn
C. Li, X. Zhou, Dr. H. Li, X. Hu
College of Materials Science and Opto-Electronic Technology
University of Chinese Academy of Sciences
Beijing 100049, P. R. China
M. Zhao, Prof. L. Shi
Department of Material Science
Fudan University
220 Handan Road, Shanghai 200433, China
E-mail: lshi@fudan.edu.cn
The ORCID identification number(s) for the author(s) of this article can be found under https://doi.org/10.1002/adom.201800651.

DOI: 10.1002/adom.201800651

 © 2018 WILEY-VCH Verlag GmbH & Co. KGaA, Weinheim

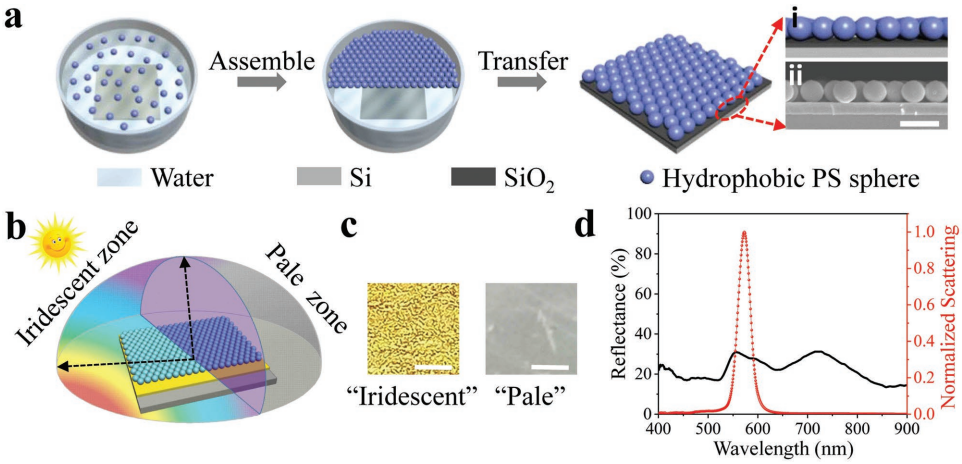

Figure 1. Janus optical response of the composite structure. a) Schematic illustration of the stepwise processes for the fabrication of the 2DPC-FP composite structure. 2D PC is assembled on the air–water interface at first and then transferred to the substrate. i and ii are the illustration (i) and the scanning electron microscope (SEM) (ii) cross-section images of 300-2DPC-FP-270. Scale bar: 1 µm. b) Schematic of optical Janus effect generated by the composite structure. c) Janus optical effect of 300-2DPC-FP-270. The composite structure shows a brilliant golden color when viewed at the same side of incident light. The pale color appears when observed at the opposite side of incident. Scale bar: 2 mm. d) Reflectance spectrum (black solid line) and normalized scattering spectrum (red dot line) of the 300-2DPC-FP-270. A sharp scattering peak at ≈570, ≈30 nm in FWHM can be clearly observed and brings the saturate yellow color. Two moderate reflection peaks ≈550 and 730 nm in the range of 400–900 nm yield the pale color.

by the composite structure. Iridophores in the skin of panther chameleons are organized into two superposed layers composite of guanine nanocrystals layer within a superficial thick layer of dermal iridophores. They can rapidly change their color by actively adjusting the lattice of the top guanine nanocrystals layer.[29] Herein, a composite architecture combining a 2D photonic crystal with a Fabry–Perot cavity (2DPC-FP) is constructed and gives rise to highly controllable hue with both high saturation and high brightness. The experimental studies and theoretical analysis are performed to find out how the composite architecture scatters the incident light and leads to high saturated coloration. Additionally, a striking Janus optical effect arises from the 2DPC-FP composite structure. A series of colors with high saturation can be obtained by designing appropriate parameters of composite structures. These asymmetrically colored materials will be of great significance in art, architecture, and security features in anticounterfeiting materials.

The facile approach to fabricate the 2DPC-FP composite structure is presented in **Figure 1**a. Silicon wafers with a SiO_2 layer, of which thickness ranges from 0 to 300 nm, are used as substrates. Own to the high refractive index and the large impedance mismatch, Si substrates work as a reflector mirror of the visible light to enhance the diffraction of the 2D PC.[30] Meanwhile, the light in the long wavelength can be absorbed by the silicon so as to reduce the random light scattering (Figure S1, Supporting Information). A polymer-spheres monolayer is firstly assembled at the air–water interface and then transferred to the substrates. The composite structure shows an obviously Janus optical effect, as shown in Figure 1b. The hemisphere presents the different color response of the 2DPC-FP composite structure: it is "iridescent" when observing from the incident light side and full-color variation shows at this side under different view angle. However, it is pale when looking from the opposite side of the incident light. From the iridescent area, a golden color is generated when the radius of the PS spheres is 300 nm, the thickness of the SiO_2 layer is 270 nm (300-2DPC-FP-270) (Figure 1c). To the naked eyes, the obtained golden color is even brighter than that of the gold film (Figure S2, Supporting Information). Scattering spectrum of the 300-2DPC-FP-270 has a peak at 570 nm, ≈30 nm in full width at half maximum (FWHM). Under identical illumination conditions, the composite structure is whitish and noniridescent when it is observed from the pale zone. The reflectance spectrum is broad ranging from 400 to 900 nm with two moderate peaks around 550 and 730 nm. The intensity of scattering is much weaker (less than 4%) than that of reflectivity (≈25%). Consequently, the color results from the reflection rather than the scattering when viewing from the pale zone. As the reflectance spectra of the composite structure is broad and have no obvious characteristic peaks, the pale color appears.

For the iridescent zone, the diffuse light produces high-contrast color flicker. **Figure 2**a displays the seven different metallic colors from purple to pink generated by the 300-2DPC-FP-270. The color gradually turns to pink from purple with the increasing view angle from ≈15° to ≈75°. Figure 2b (IsoPlane SCT320) shows the white reflection spot and the first-order diffraction spots when the incident angle is 25°. It clearly shows that the reflection spot is white while the diffraction spots are colorful. The discrepant coloration of spots demonstrates the Janus structural color response of the composite structure. The reflection spot with two diffraction spots forms an equal-lateral triangle because a hexagonal pattern of spots is created by the diffraction of the composite structure. The six spots correspond to the six reciprocal lattice vectors of the 2D close-packed hexagonal particle array (Figure S3, Supporting Information).[31] Figure 2c is the scattering spectra of the iridescent zone when the light incidents at 25°. According to the spectra, the 2DPC-FP composite structure exhibits red-shifting scattering peaks from ≈400 nm (purple) to 630 nm (pink) under different receiving angles from 18°–48°. The FWHMs of these scattering peaks are ≈30 nm. It is the sharp and narrow peaks

© 2018 WILEY-VCH Verlag GmbH & Co. KGaA, Weinheim

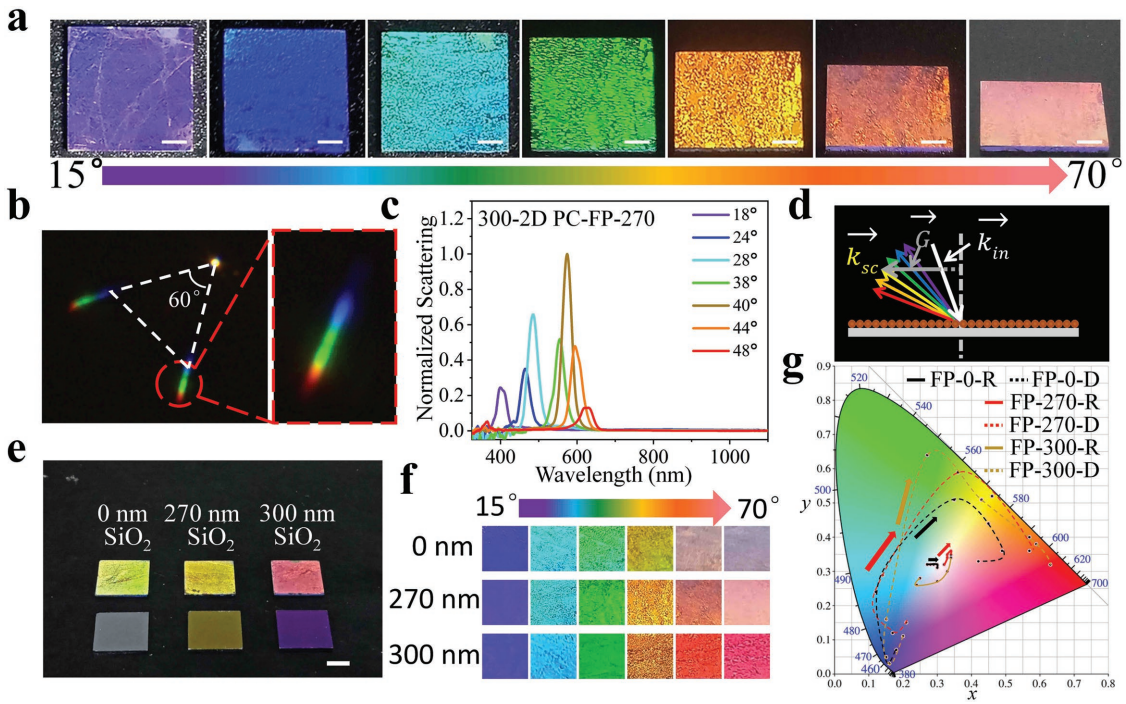

Figure 2. Diversified colors generated by different composite structures. a) Optical photos of different colors brought by the 300-2DPC-FP-270 when incident under ≈25°. Scale bar: 2 mm. b) The first-order diffraction photos of the 2DPC-FP composite structure under 25° incident. Red rectangle is an enlarged diffraction spot. The white spot derives from reflection. Three spots can form an equal-lateral triangle because of the hexagonally packed structure of 2D PC. c) Scattering spectra under ≈25° incident of the 2DPC-FP composite structure corresponding to the colors in (a), respectively. It is the sharp and narrow peaks that bring the vivid metallic colors in the iridescent zone. d) The first-order diffraction schematic of the 2DPC-FP composite structure. Scattering light is red shifting with increasing scattering angle. e) Contrast of different structures, including different substrates and different composite structures. The difference in coloration manifests the manipulation from the composite structure. f) A palette obtained by 300-2DPC-FP-0, 300-2DPC-FP-270, and 300-2DPC-FP-300. g) Chromaticity coordinates of the 2DPC-FP composite structures in (f). The solid lines correspond to reflection spectrum when the dot lines are consistent with the scattering spectra of 300-2DPC-FP-0 (black), 300-2DPC-FP-270 (red), and 300-2DPC-FP-300 (golden), respectively. Broader color gamut yields by the scattering lines than that by the reflectance. It indicates that the scattering of the composite structure can bring more vivid colors than the reflection.

that yield the saturated structure colors. To the naked eyes, the colors result from those scattering peaks are also high contrast and glaring because of the weak background noises generated by the scattering.[32,33]

Meanwhile, the color can be tuned by changing the thickness (t) of the SiO_2 coating and the radius of the PS spheres (R). As shown in Figure 2d, the basic configuration of the color pixel consists of a dielectric oxide layer and a closely-packed monolayer of colloid spheres. The configuration forms a resonance cavity combining the 2D PC and the FP film. The color gamut of the composite structure is closely linked with the particle spacing and the refractive index of the 2D PC.[31] In addition, the thickness of the FP cavity layer in the composite structure is also important to the colors. Figure 2e shows the colors of different structures, including different bare substrates and composite structures. The color difference between these structures indicates a unique manipulation of light from the resonance cavity. Furthermore, different metallic colors can be obtained under different view angles, offering a color palette as shown in Figure 2f. According to the palette, the structure without SiO_2 layer exhibits colors from pure purple to dim pink. The coloration's saturation is decreasing with increasing view angle. The 300-2DPC-FP-270 can produce colors from pure purple to pink. Among them, the yellow color is bright and vivid. The 300-2DPC-FP-300 can yield colors from purple to red. Both green and red colors are brilliant metallic texture. In Figure S4 (Supporting Information), it is found that the scattering peak intensity is vulnerable by the thickness of the SiO_2 layer. To study the color variation with the view angle and the thickness of the FP film, the measured scattering and reflection spectra of these three structures are converted into the Commission International de l'Eclairage (CIE) chromaticity values, shown in Figure 2g. The solid lines plot on the chromaticity diagram corresponds to the color generated by specular reflection under different view angles, and the dot lines are consistent with the scattering spectra (Figure S4, Supporting Information). The color gamut of the reflection of 2DPC-FP composite structures is much smaller than that of their scattering, as shown in Figure 2g. The difference between CIE indicates that the scattering can produce more vivid colors than the reflection. According to the CIE diagram, the yellow color CIE value (0.46, 0.52, 0.02) generated by the 300-2DPC-FP-270 is very close to the pure yellow (0.46, 0.53, 0). In the meantime, the CIE of the red color (0.63, 0.32, 0.05) caused by the 300-2DPC-FP-300 is close to the CIE of the pure red (0.73, 0.26, 0). It is worth noticing that the blue color caused by these three structures hardly changes, which is resulted from the Rayleigh scattering.[34] Multi-interaction between light and composite

© 2018 WILEY-VCH Verlag GmbH & Co. KGaA, Weinheim

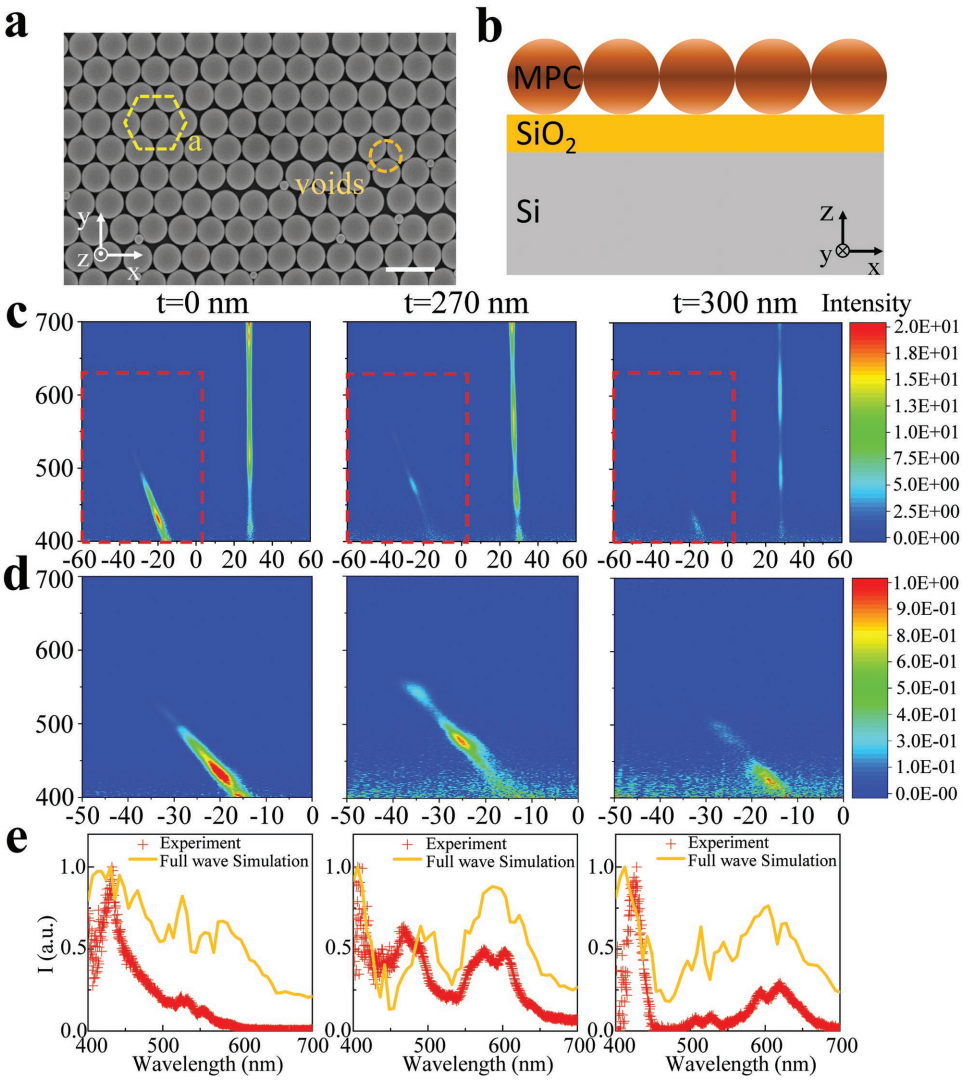

Figure 3. Diffraction and simulation of different 2DPC-FP composite structure. a) Top-view SEM image of 300-2DPC-FP-270. The yellow dot hexagon denotes the hexagonal dense packing of spheres on the *x*–*y* plane and *a* is the lattice constant. The orange dot ring shows the voids between microspheres with the size ≈100 nm. Scale bar: 1 µm. b) Realistic model of the 2DPC-FP composite structure. The light is diffracted by the 2D PC to generate colors. The bottom film can enhance the diffracted color when the constructive interference happens. c) Diffraction and reflection images of 300-2DPC-FP-0, 300–2DPC-FP-270, and 300-2DPC-FP-300, respectively. The red dot rectangles denote the diffraction images. d) Normalized diffraction images, which are noted by the red dot rectangle in (c). e) Contrast between the experimental results (red) and FDTD simulations of scattering peak's intensity based on the realistic model (yellow). Obvious regulation exhibits when the FP layer is introduced.

structure leads to the different color saturation. Figure S5 (Supporting Information) shows different metallic coloration of three 2DPC-FP composite structures of 300-2DPC-FP-0, 300-2DPC-FP-270, and 300-2DPC-FP-300. In accordance with the CIE diagram, different color has been approved at the long wavelength, which is more susceptible by the bottom FP layer compared with the colors at short wavelength.

To further study the effect of the 2DPC-FP composite structures on the coloration, we simulate the propagation of light in the composite structure by finite-difference time domain method (FDTD, **Figure 3**). Figure 3a is the scanning electron microscope (SEM) image of the 300-2DPC-FP-270. It clearly shows that the spheres are hexagonal closely packed. The lattice constant of this structure is *a*. As a result, the reciprocal lattice vectors of the film are $\frac{2\pi}{a}$ on the *x*–*y* plane. For the simulation, the actual composite structure based on SEM images is used. When the composite structure is illuminated, the light will be scattered by the PS spheres into all directions. There are two optimal modes for the light propagation. One is the diffraction mode resulting from the reciprocal lattice vectors with proper incident and scattering angle. When the light is scattered onto the FP layer, the interference mode occurs. Diffraction is enhanced when the constructive interference happens, which closely links to the material of microspheres and FP cavity. Figure 3c shows the experimental diffraction images of the 2DPC-FP composite structure of 300-2DPC-FP-0, 300-2DPC-FP-270, and 300-2DPC-FP-300. The normalized diffraction images are shown in Figure 3d. Disparity between three structures is obvious. To compare the diffraction induced by different composite structure more intuitively, the normalized scattering intensity curves of different wavelengths

© 2018 WILEY-VCH Verlag GmbH & Co. KGaA, Weinheim

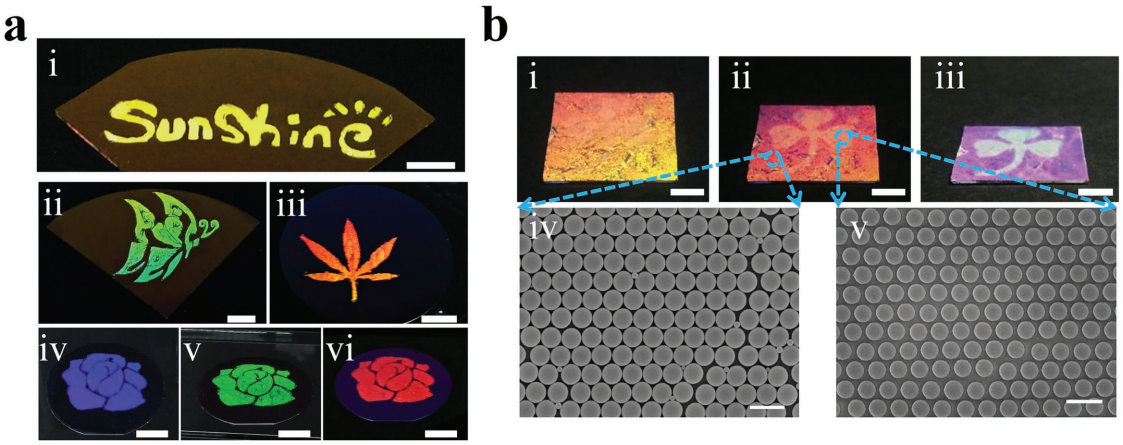

Figure 4. Patterns and anticounterfeiting applications of 2DPC-FP composite structures. a) Various images are prepared by 300-2DPC-FP-270 and 300-2DPC-FP-300. i,ii) Golden word "sunshine" and iridescent butterfly made by 300-2DPC-FP-270. iii–vi) "Maple leaf" and flower with different colors generated by the 300-2DPC-FP-300. Scale bar: 1 cm. b) Anticounterfeiting clover pattern on the composite structure. The pattern can be hidden at small view angles (i) but gradually exhibits when increasing view angles (ii,iii). Scale bar: 5 mm. Insets are SEM images of PS microspheres in the untreated area (300 nm, iv) and clover area (250 nm, v). It is the distinction of spheres size that lead to the angle-dependent anticounterfeiting material. Scale bar: 1 μm.

are shown in Figure 3e (red curves). FDTD simulation results of the realistic composite structures (yellow curve) of diffraction intensity at different wavelength are also shown in Figure 3e. It shows that the simulation results of the realistic composite structure are in agreement with the experimental ones quite well. The difference between simulations and experiments is mainly because that the 2D PC is not always closely packed as shown in Figure 3a. For the 300-2DPC-FP-0, only one broad peak exists at ≈425 nm in the visible-light range. This demonstrates that a strong diffraction occurs here. Consequently, the colors with spectra peak ≈425 nm, such as blue, is more saturated and brighter than the others (Figure 2f). On the other hand, there are two peaks in the diffraction intensity curve when the FP film is introduced into the structure. It indicates a significant regulation of the diffraction strength at different wavelength from the composite structure, leading to the fact that the composite structure reported here have more degree of freedom to tune and control the observed structural color. For the 300-2DPC-FP-270, strong diffraction happens at ≈500 nm and ≈580 nm. When the thickness of SiO_2 layer is increased to 300 nm, strong diffraction happens at ≈400 nm and ≈600 nm. As a result, more saturated yellow metallic color can be yield by the 300-2DPC-FP-270 contrast to the 300-2DPC-FP-0. Meanwhile, a better metallic red color is produced by the 300-2DPC-FP-300 than that by the 300-2DPC-FP-0 (Figure S5, Supporting Information). However, the blue color generated by the three structures are similar. This is mainly because at the short wavelength, the light is not only adjusted by the interference, but also significantly influenced by the Rayleigh scattering owing to the voids between microspheres (≈100 nm in size) (Figure 2b-ii). According to the Rayleigh scattering, the intensity of scattering is inversely proportional to the fourth power of the wavelength (λ^4). As a result, the short wavelength light is dominated by the Rayleigh scattering. Thus, the colors at short wavelength are substrate-insensitive. The diffraction intensity of composite structure with different sphere size is also simulated, as shown in Figure S6 (Supporting Information). According to the simulation, the diffraction wavelength that is enhanced by the composite structure is constant when increasing the size of the spheres. However, the range of diffracted wavelength is expanded when increasing the sphere size. It powerfully demonstrates that the bottom interference layer dominates the regulation of the color. It is noticable that the diffraction intensity decreases based on the simulation results of free-standing symmetric sphere arrays when the Si substrates is abscent (Figure S7, Supporting Information). It clearly shows the impact of the silicon substrate.

Angle-sensitive structural color is very prevalent in nature. Many creatures use their color to protect themselves from the predators by hiding in surrounding or to attract focus through brilliant colors. Similarly, the angle-dependent color pixels based on 2DPC-FP composite structure also have significant potential application for camouflage and anticounterfeiting applications. **Figure 4** shows a sort of vivid images. In these examples, all the patterns are viewed from the iridescent zone. In this way, high saturation patterns with single color or gradient colors can be obtained. Via constructing composite structure of 300-2DPC-FP-270, the pure glaring "yellow sunshine" and gradient iridescent butterfly are produced. Orange "maple" and pure color "flower" can be made by changing the thickness of the SiO_2 layer to 300 nm. What is more, a realistic anticounterfeiting application is demonstrated by designing a pattern via changing the size of 2D PC. In Figure 4b, the clover pattern is hidden when observed at a small angle, but it gradually appears when increasing the view angle. The pattern is fabricated by plasma etching. SEM images in Figure 4b demonstrate that the PS microspheres of the clover (R = 250 nm) are smaller than those in the untreated area (R = 300 nm) due to plasma etching. But the particle spacing is constant for two areas. The scattering spectra of these two areas are measured as shown in Figure S8 (Supporting Information). The scattering peaks generated by two areas are too similar to distinguish them when the sample is observed at a small view angle (Figure S8a, Supporting Information). As a result, the pattern is invisible. When increasing the viewing angle, the clover pattern produces a stronger scattering than

© 2018 WILEY-VCH Verlag GmbH & Co. KGaA, Weinheim

that of untreated area. This mainly results from the synergistic effect of the interference and Raleigh scattering. To contrast the relative scattering strength between two areas, the ratio of $\Delta I/I_0$ is introduced. The ΔI is the difference of scattering intensity between two areas. The I_0 is the scattering intensity of the untreated area. When the viewing angle is increasing, the ratio is also raising from 0.2 to 1.6 (Figure S8b, Supporting Information). This indicates that the pattern is gradually appearing. Consequently, the angle-dependent anticounterfeiting material can be prepared by designing 2DPC-FP composite structure. To demonstrate the Janus color response of the 2DPC-FP composite structure, the butterfly pattern and the anticounterfeiting glove pattern are photographed at both sides, as shown in Figure S9 (Supporting Information). The patterns manifest dim pale color at the opposite side of the incident light.

In summary, we construct a 2DPC-FP composite structure through a facile low cost method that suits for various substrates and large-scale preparation. By assembling monolayer photonic crystal on FP cavity coating substrates, an optical Janus effect can be produced wherein the color is different on the same side of the incident light than that on the opposite side. It is easy to tune the hues and saturation of the colors by adjusting the lattice constant of 2D PC and the thickness of the SiO_2 layer. The coloration is derived from the synergistic effect of the interference, the diffraction, and the Raleigh scattering of the composite structure. Both experiments and simulations indicate that the composite structures can provide much more opportunities to obtain diversified colors. This 2DPC-FP composite structure is very promising in traditional areas, such as the art, architecture, and security feature in anticounterfeiting materials. In addition, the compositization of multistructures is also an approach to make bionic chameleons skins.

Experimental Section

2DPC-FP Composite Structure Fabrication: The 2D PC was assembled on the SiO_2-Si substrate by the following steps: at first, 10 wt% PS microspheres colloidal solution and deionized water as well as ethanol were mixed with the volume ratio 1:1:2. Different SiO_2-Si wafers were pretreated by Piranha solution (H_2SO_4:H_2O_2 = 7:3, volume ratio) and heated for 2 h, followed by putting the pretreated substrates in a clean Petri dish, and pouring in the right amount of water. Then the PS solution was dripped onto the air–water interface. PS spheres would form a monolayer film at the water–air interface due to hydrophobicity of the spheres and volatility of ethanol. SDS solution was used in the end to obtain a more orderly closely packed monolayer film. The 2D PC was transferred to Si substrate by sucking out extra water carefully. The 2DPC-FP composite structure is obtained after putting the film into 80 °C oven drying for 30 min.

Structural Color Patterns: The patterns were obtained by the plasma etching with different mask.

Characterization: Optical graphs were captured by a digital camera (EOS 700D, Canon). Scattering spectra were mearsured by angle-resolved spectrum system (ideaoptics, China) equipped with a high sensitive spectrometer (NOVA, ideaoptics, China). SEM images of composite structure were taken by a field emission scanning electron microscope (JSM-7500F, Japan). Diffraction images were conducted by isoplane spectrometer (SCT320, Preceton). CIE diagram was converted by the Matlab.

Supporting Information

Supporting Information is available from the Wiley Online Library or from the author.

Acknowledgements

C.L. and M.Z. contributed equally to this work. This work was supported by the National Natural Science Foundation of China (Grant No. 21522308, 51573192, 51773206, 51473173, 11774063, 11727811), External Cooperation Program of BIC, Chinese Academy of Sciences, Grant No. 121111KYSB20150022, Youth Innovation Promotion Association CAS and Technology Commission of Shanghai Municipality (17142200100). All the authors gratefully acknowledge Ideaoptics Inc. and Dr. Haiwei Yin as well as M.S. Zhenghong Li for their valuable discussion and kind helps in characterizing the optical properties of the films.

Conflict of Interest

The authors declare no conflict of interest.

Keywords

2D photonic crystals, anti-counterfeiting, Fabry–Perot cavities, high saturation, structural colors

Received: May 16, 2018
Revised: June 27, 2018
Published online:

[1] P. Vukusic, J. R. Sambles, *Nature* **2003**, *424*, 852.
[2] T. Starkey, P. Vukusic, *Nanophotonics* **2013**, *2*, 289.
[3] Z. Yang, Y. Chen, Y. Zhou, Y. Wang, P. Dai, X. Zhu, H. Duan, *Adv. Opt. Mater.* **2017**, *5*, 1700029.
[4] J. X. Wang, L. B. Wang, Y. L. Song, L. Jiang, *J. Mater. Chem. C* **2013**, *1*, 6048.
[5] Y. Y. Diao, X. Y. Liu, G. W. Toh, L. Shi, J. Zi, *Adv. Funct. Mater.* **2013**, *23*, 5373.
[6] Z. Cai, J.-T. Zhang, F. Xue, Z. Hong, D. Punihaole, S. A. Asher, *Anal. Chem.* **2014**, *86*, 4840.
[7] H. Wang, K.-Q. Zhang, *Sensors* **2013**, *13*, 4192.
[8] D. P. Puzzo, A. C. Arsenault, I. Manners, G. A. Ozin, *Angew. Chem., Int. Ed.* **2009**, *121*, 961.
[9] A. C. Arsenault, D. P. Puzzo, I. Manners, G. A. Ozin, *Nat. Photonics* **2007**, *1*, 468.
[10] J. Hou, H. Zhang, B. Su, M. Li, Q. Yang, L. Jiang, Y. Song, *Chem. - Asian J.* **2016**, *11*, 2680.
[11] S. Kinoshita, S. Yoshioka, J. Miyazaki, *Rep. Prog. Phys.* **2008**, *71*, 076401.
[12] Z. Yang, Y. Zhou, Y. Chen, Y. Wang, P. Dai, Z. Zhang, H. Duan, *Adv. Opt. Mater.* **2016**, *4*, 1196.
[13] L. Duempelmann, A. Luu-Dinh, B. Gallinet, L. Novotny, *ACS Photonics* **2016**, *3*, 190.
[14] L. Duempelmann, D. Casari, A. Luu-Dinh, B. Gallinet, L. Novotny, *ACS Nano* **2015**, *9*, 12383.
[15] M. Burresi, L. Cortese, L. Pattelli, M. Kolle, P. Vukusic, D. S. Wiersma, U. Steiner, S. Vignolini, *Sci. Rep.* **2014**, *4*, 6075.
[16] J. Syurik, G. Jacucci, O. D. Onelli, H. Hölscher, S. Vignolini, *Adv. Funct. Mater.* **2018**, 1706901.
[17] H. Kim, J. Ge, J. Kim, S.-e. Choi, H. Lee, H. Lee, W. Park, Y. Yin, S. Kwon, *Nat. Photonics* **2009**, *3*, 534.

© 2018 WILEY-VCH Verlag GmbH & Co. KGaA, Weinheim

[18] J. Ge, J. Goebl, L. He, Z. Lu, Y. Yin, *Adv. Mater.* **2009**, *21*, 4259.
[19] F. Fua, Z. Chena, Z. Zhaoa, H. Wanga, L. Shanga, Z. Gua, Y. Zhao, *Proc. Natl. Acad. Sci. USA* **2017**, *114*, 5900.
[20] M. Elbahri, M. e. Abdelaziz, S. Homaeigohar, A. Elsharawy, M. Keshavarz Hedayati, C. Röder, M. El Haj Assad, R. Abdelaziz, *Adv. Mater.* **2018**, *30*, 1704442.
[21] T. Chen, B. M. Reinhard, *Adv. Mater.* **2016**, *28*, 3522.
[22] G. T. England, J. Aizenberg, *Rep. Prog. Phys.* **2018**, *81*, 016402.
[23] C. Ji, K.-T. Lee, T. Xu, J. Zhou, H. J. Park, L. J. Guo, *Adv. Opt. Mater.* **2017**, *5*, 1700368.
[24] Y. Zhang, B. Dong, A. Chen, X. Liu, L. Shi, J. Zi, *Adv. Mater.* **2015**, *27*, 4719.
[25] G. T. England, C. Russell, E. Shirman, T. Kay, N. Vogel, J. Aizenberg, *Adv. Mater.* **2017**, *29*, 1606876.
[26] M. D. Shawkey, N. I. Morehouse, P. Vukusic, *J. R. Soc., Interface* **2009**, *6*, S221.
[27] M. Kolle, P. M. Salgard-Cunha, M. R. Scherer, F. Huang, P. Vukusic, S. Mahajan, J. J. Baumberg, U. Steiner, *Nat. Nanotechnol.* **2010**, *5*, 511.
[28] A. R. Parker, Z. Hegedus, *J. Opt. A: Pure Appl. Opt.* **2003**, *5*, S111.
[29] J. Teyssier, S. V. Saenko, D. Van Der Marel, M. C. Milinkovitch, *Nat. Commun.* **2015**, *6*, 6368.
[30] A. Tikhonov, N. Kornienko, J. T. Zhang, L. L. Wang, S. A. Asher, *J. Nanophotonics* **2012**, *6*, 063509.
[31] S. A. Asher, J. M. Weissman, A. Tikhonov, R. D. Coalson, R. Kesavamoorthy, *Phys. Rev. E* **2004**, *69*, 066619.
[32] J. Steinhardt, *J. Gen. Physiol.* **1936**, *20*, 185.
[33] S. Hecht, J. C. Peskin, M. Patt, *J. Gen. Physiol.* **1938**, *22*, 7.
[34] D. Ge, L. Yang, G. Wu, S. Yang, *J. Mater. Chem. C* **2014**, *2*, 4395.

© 2018 WILEY-VCH Verlag GmbH & Co. KGaA, Weinheim